SEDIMENTOLOGY the journal of the International Association of Sedimentologists IAS

Sedimentology (2026) doi: 10.1111/sed.70078

Recycling control on chemical weathering indices (Yarlung River, South Tibet)

WENDONG LIANG*, XIUMIAN HU†, ZITING ZHAO* and EDUARDO GARZANTI‡

**State Key Laboratory of Oil and Gas Reservoir Geology and Exploitation, Institute of Sedimentary Geology, Chengdu University of Technology, 610059, Chengdu, China (E-mail: liangwendong09@163.com)*

†School of Earth Sciences and Engineering, Nanjing University, 210023, Nanjing, China (E-mail: huxm@nju.edu.cn)

‡Laboratory for Provenance Studies, Department of Earth and Environmental Sciences, University of Milano-Bicocca, 20126, Milan, Italy

Associate Editor: Zhifei Liu

ABSTRACT

Geochemical proxies are widely considered to effectively reflect weathering intensity across drainage basins, without duly considering the possibility that weathering features can be inherited from previous sedimentary cycles. To elucidate the impact of the recycling effect on weathering assessments, this study investigates sandbar and suspended sediments in the Yarlung River, representing the Tibetan headwaters of the Brahmaputra River, by comparing weathering proxies in largely first-cycle sediments derived from igneous rocks of the Lhasa Block versus overwhelmingly recycled sediments from sedimentary rocks of the Himalayan belt. First-cycle sediments record modern weathering intensity, whereas recycled sediments reflect an integrated weathering history incorporating also chemical effects acquired during previous sedimentary cycles. Detritus derived from the Himalayan belt thus misleadingly appears to be more weathered than detritus shed from the Lhasa Block in the same modern semiarid climate. Weathering signatures in the Yarlung catchment are thus primarily governed by grain-size controlled variability in sediment contribution from the Lhasa Block versus Himalayan belt. Because of the inherited weathering signals, recycled sediments systematically have higher CIA and lower WIP than first-cycle sediments, a discrepancy particularly manifest under lower temperature and precipitation conditions. Because all major rivers flow across sedimentary basins, recycled detritus is abundant in deltaic to turbiditic sediments and sedimentary rocks worldwide. This implies that the weathering signal they carry is invariably the sum of weathering acquired in the catchment plus paleo-weathering. Detangling coeval versus inherited weathering effects poses a fundamental challenge in sedimentary research if reliable climatic and paleoclimatic reconstructions must be obtained.

Keywords chemical indices, grain-size control, paleo-weathering, recycling effect, weathering intensity.

INTRODUCTION

River sediments generated under diverse climatic and tectonic conditions are widely used to assess weathering intensity at continental scale (e.g., Li & Yang, 2010; Shao *et al.*, 2012; Clift *et al.*, 2014; Yang *et al.*, 2016; Hameed & Srivastava, 2025). Studies of modern river catchments have considerably helped to better understand the present environmental evolution in a period of global

warming, providing fundamental references for paleoclimate reconstructions as well as for more reliable predictions of future climate trends (Garzanti & Resentini, 2016; White & Brantley, 2018). Geochemical proxies are most extensively applied to evaluate silicate weathering, including ratios [e.g., SiO_2/Al_2O_3 (Ruxton, 1968), K/Na and Al/Na (Yang *et al.*, 2004), Rb/Sr and Ba/Sr (Chen *et al.*, 1999; Yang *et al.*, 2004), α^{Al} values (Gaillardet *et al.*, 1999; Garzanti *et al.*, 2013)], multi-element indices [e.g., CIA (Nesbitt & Young, 1982), PIA (Fedo *et al.*, 1995) and WIP (Parker, 1970)], or trace elements (e.g., REEs; Guo *et al.*, 2025). However, being dependent on several factors (Shao *et al.*, 2012; Guo *et al.*, 2018), all of these proxies have considerable limitations even in the study of modern sediments (e.g., Deng *et al.*, 2022; Guo *et al.*, 2022), leading to potentially serious misinterpretations in paleoclimate reconstructions (e.g., Li & Yang, 2010; Fu *et al.*, 2023). The mineralogical and chemical composition of siliciclastic sediments is markedly dependent on grain size, sediment recycling, and hydraulic sorting during transport and deposition, all factors that can compromise accurate weathering assessments (Fedo *et al.*, 1995; Bouchez *et al.*, 2011; von Eynatten *et al.*, 2016; Joo *et al.*, 2018; Garzanti *et al.*, 2025a).

Studies of dissolved loads in river basins have highlighted the effect of the chemical composition of source rocks on weathering rates (Bluth & Kump, 1994), an effect still understudied in sediments (Gaillardet *et al.*, 1999; Li & Yang, 2010; Dellinger *et al.*, 2017). One particularly underestimated factor is that sedimentary and low-grade metasedimentary rocks, widely occurring in most river basins, invariably incorporate the effects of multiple earlier weathering cycles; the detritus they shed thus invariably archives their integrated weathering history (e.g., Garzanti *et al.*, 2022, 2025b). Weathering indices of riverine solid materials do not only reflect the current weathering regime, but also multiple chemical effects of paleo-weathering and diagenesis acquired during potentially numerous previous sedimentary cycles (e.g., Gaillardet *et al.*, 1999; Dellinger *et al.*, 2017). The relationship between weathering indices of polycyclic sedimentary products and climatic regimes is therefore complex.

Although numerous case studies have recognised that sediment recycling introduces biases (Borges *et al.*, 2008; Guo *et al.*, 2018; Garzanti *et al.*, 2019, 2022; Fu *et al.*, 2023), no current research has focused strictly on the impact of sediment recycling on basin-wide weathering assessments. Researches have shown that the progressive concentration of durable minerals through multiple sedimentary cycles significantly impacts the applicability of chemical indices sensitive to quartz dilution (e.g., WIP), whereas the CIA and α^{Al}_{Na} are not affected by mere quartz addition (Garzanti *et al.*, 2013; Yang *et al.*, 2016; Dinis *et al.*, 2017; Guo *et al.*, 2018). The main crux remains the conceptual and practical difficulty in the recognition of weathering features inherited from previous cycles and their distinction from newly acquired effects in the last sedimentary cycle. This uncertainty raises questions about the potential decoupling between measured chemical weathering indices and actual climatic conditions.

Suspended and sandbar sediments are common media for assessing weathering intensity in river catchments. Suspension sorting during transport—controlled by the relationships among grain size, density, and shape of different detrital minerals—induces compositional partitioning between suspended load and bedload (Bouchez *et al.*, 2011; Garzanti *et al.*, 2011; Lupker *et al.*, 2011). This factor inevitably impacts on weathering evaluations.

To address these issues, we here conduct geochemical tests and weathering assessments on different grain-size fractions of suspended and sandbar sediments from the Yarlung River (Tibetan headwaters of the Brahmaputra). Previous studies in the Yarlung River attributed the silicate weathering intensity to climatic variations (Yu *et al.*, 2025; Zhao *et al.*, 2025), without considering the recycling effect. By combining lithological information with temperature and precipitation data, we explore the controlling factors of weathering processes in the region and circumstantiate the response of weathering indices in first-cycle versus recycled detritus. Furthermore, by comparing weathering indices of fine-grained river sediments of small- and median-sized catchments at the global scale (Deng *et al.*, 2022), we investigate the influence of sediment recycling in different settings and highlight the implications of recycling effects on the perceived weathering intensity and the pitfalls involved.

HYDROLOGICAL AND GEOLOGICAL BACKGROUND

Drainage system

The Yarlung River originates from the Chamyungdung glacier on the northern slope of the

Himalayan Mountains and flows eastward for over 2000 km along the India/Asia suture zone until it plunges into the deep gorges across the Namche Barwa syntaxis (Fig. 1). The Yarlung catchment area is ~2.4 × 10^5 km^2, the mean altitude is above 4000 m, and the average equilibrium slope is 2.6‰. The catchment is here subdivided into three parts: the upper reaches upstream of the Lhatse hydrological station, the middle reaches between the Lhatse and Nuxia stations, and the lower reaches between Nuxia and the gorges (Fig. 1B).

Because of the rain-shadow effect caused by the high relief of the Himalayan Mountains, the climate of the Yarlung catchment is semiarid and modulated by the Indian summer monsoon, which penetrates in the region primarily *via* the Yarlung River gorge. Summer rainfall and temperature thus systematically increase from west to east (Bookhagen & Burbank, 2006), and

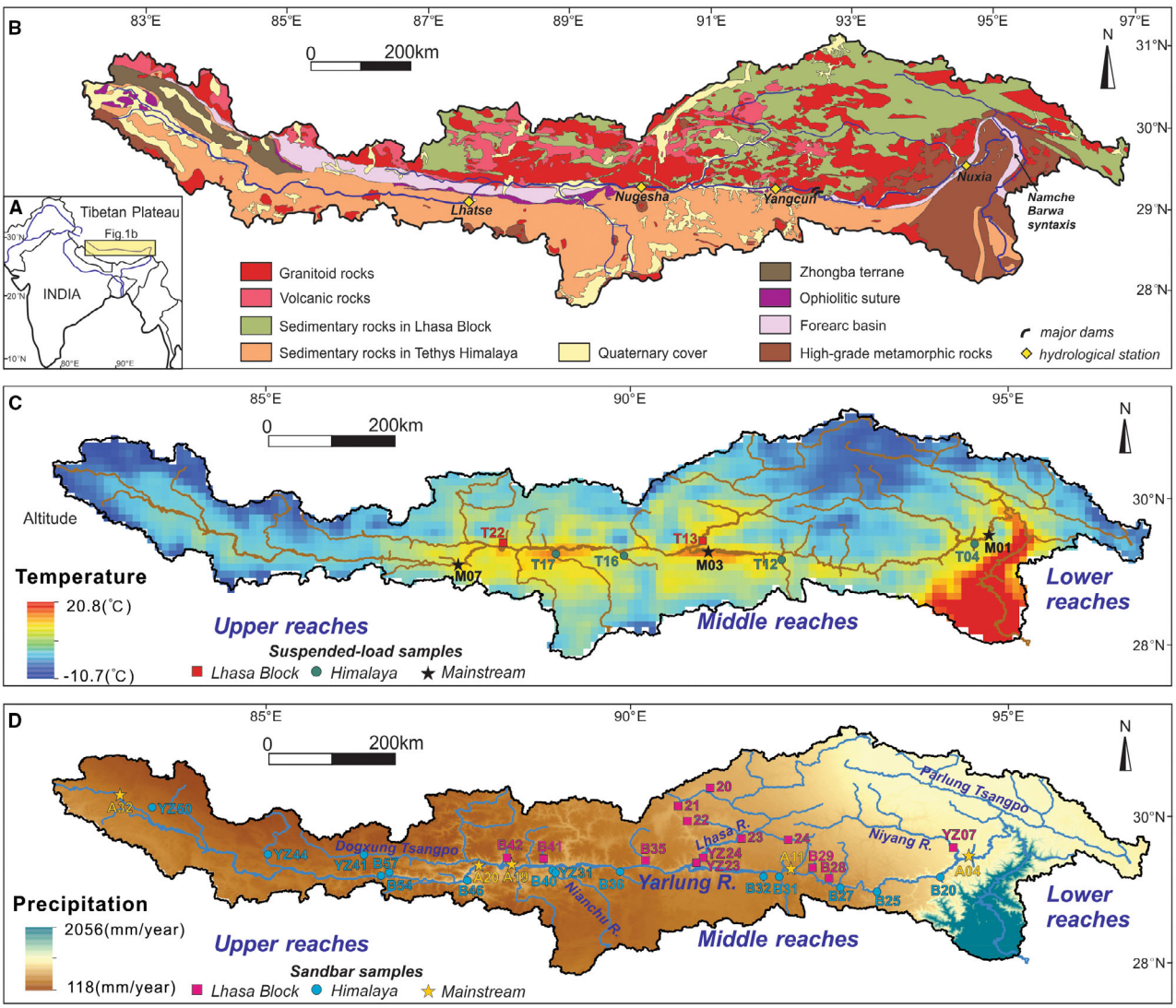

Fig. 1. The Yarlung River (*Yarlung Tsangpo* in Tibetan language). (A) Geographic location. (B) Geological map (modified after Pan *et al.*, 2004). (C) Mean annual temperature (MAT; from 2013 to 2022, after Muñoz, 2019) and suspended samples. (D) Mean annual precipitation (MAP; from 2012 to 2021; after Peng, 2024) and sandbar samples, including 20, 21, 22, 23 and 24 from tributaries draining Lhasa Block granitoids (selected from Zhao *et al.*, 2025), YZ07, YZ23, YZ24 representing Lhasa Block sediments, and YZ31, YZ41, YZ44 and YZ50 representing Himalayan sediments (selected from Yu *et al.*, 2025).

climate exerts a similar influence on both southern Himalayan and northern Tibetan sides of the river course (Fig. 1C,D). In the wet season (from June to September), the northward shift in the Indian monsoon accounts for 60 to 80% of the annual precipitation.

Geological setting

The Yarlung catchment comprises three major tectonic domains: the northern part of the Himalayan belt in the south (Tethys Himalaya), the Lhasa Block in the north, and the India/Asia suture zone in between (Fig. 1B). The Tethys Himalaya primarily consists of a Palaeozoic to Eocene sedimentary succession in the southern proximal part, chiefly including deltaic to shelfal siliciclastics and platform to pelagic carbonates, and Mesozoic to Palaeocene outer shelf, continental slope, and rise deposits in the northern distal part (Sciunnach & Garzanti, 2012; Hu *et al.*, 2016a). The southern tributaries of the Yarlung River also drain North Himalayan gneiss domes with their surrounding metamorphic aureole and Miocene leucogranites intruded into the high-grade Greater Himalaya metamorphic rocks exposed along the southern edge of the catchment (Carosi *et al.*, 2019). The Lhasa Block is further subdivided into southern, central, and northern terranes. The southern Lhasa terrane includes the Gangdese arc batholith, Jurassic–Eocene volcanic rocks, and Upper Triassic–Cretaceous sedimentary rocks (Zhu *et al.*, 2013). The central Lhasa terrane contains very low-grade Upper Palaeozoic metasedimentary rocks and Upper Jurassic–Lower Cretaceous volcanic and sedimentary rocks. The northern Lhasa terrane comprises Cretaceous, Jurassic, and Triassic sedimentary rocks (Zhu *et al.*, 2011). The contrasting petrological and heavy-mineral characteristics of the Yarlung tributaries draining the Lhasa Block and the Himalayan belt are illustrated in detail in Liang *et al.* (2020, 2022, 2025). The suture zone along which the Yarlung River flows represents the upper-plate edge of the India-Asia collision (An *et al.*, 2014; Hu *et al.*, 2015), including the ophiolitic basement of the Xigaze forearc basin filled by upper Lower Cretaceous to Eocene turbidites and deltaic siliciclastic rocks (Hu *et al.*, 2016b; Wang *et al.*, 2017). Because of its limited exposure area, the suture zone contributes marginally to the Yarlung sediment load (Liang *et al.*, 2022, 2025) and can be disregarded for the purposes of the present study.

MATERIALS AND METHODS

Samples collected from active fluvial sandbars in November 2019 and suspended sediment collected at the channel's midpoint during June–July 2023 have been studied by Liang *et al.* (2022) and Liang *et al.* (2025), respectively. Eight selected sandbar samples and nine suspended sediments from the mainstem and tributaries were selected for this study. As fine-grained sediments tend to contain more silicate weathering characteristics, and selecting a narrow size window can reduce the influence of hydraulic sorting, we conducted wet sieving on these samples to obtain their mud fractions (<63 μm). Following a lithium metaborate fusion and nitro-hydrochloric acid digestion, major oxides in the 17 mud fractions were determined with a HORIBA ULTIMA 2C ICP-MS at Nanjing Hongchaung Geological Exploration Technology Service Co., Ltd. (data provided in Table S1). The geochemical composition of clay fraction (<2 μm; Yu *et al.*, 2025), mud fraction (<63 μm; Yu *et al.*, 2025; Zhao *et al.*, 2025), sand fraction (63 to 2000 μm; Liang *et al.*, 2022), and of the <2000 μm fraction (Wu *et al.*, 2012; Zhang *et al.*, 2021; Liang *et al.*, 2022) were considered for comparison (Table S2).

The Chemical Index of Alteration [CIA = $100 \times A1_2O_3/(A1_2O_3 + CaO^* + Na_2O + K_2O)$; Nesbitt & Young, 1982] and the Weathering Index [WIP = $100 \times (CaO/0.7 + 2Na_2O/0.35 + 2K_2O/0.25 + MgO/0.9)$; Parker, 1970] are widely used to estimate weathering intensity. CaO is CaO associated with the silicate fraction only, assumed to be equal to Na_2O in case CaO moles are greater than Na_2O moles after correcting for CaO in apatite (McLennan, 1993). The Chemical Index of Quartz-enrichment [CIQ = $(172.4 - 1.7 \times CIA - WIP)/WIP$; Guo *et al.*, 2024] was also calculated to better assess the hydrodynamic sorting and sedimentary recycling. Weathering intensity can be evaluated separately for each single mobile element by α^{Al} values [$\alpha^{Al}E = (Al/E)_{sample}/(Al/E)_{UCC}$; Garzanti *et al.*, 2013], which compare the concentrations of mobile element *E* with nonmobile Al in our samples and in the upper continental crust (UCC; Taylor & McLennan, 1995; Rudnick & Gao, 2003). Key geochemical parameters and weathering indices are shown in Table S2.

RESULTS

In the Yarlung catchment, suspended sediment has lower SiO_2 (56.9% on average) and higher Al_2O_3 (17.7%) and K_2O (3.5%) than sandbar sediment (SiO_2 66.0%, Al_2O_3 13.5%, and K_2O 2.2% on average). Other major elements are less variable (Fe_2O_3 6.7%, CaO 3.0%, MgO 2.0%, and Na_2O 2.0% on average; Table S1). Greater differences exist between suspended load and sandbar sediments in Himalayan tributaries (SiO_2 55.3% versus 68.3% and Al_2O_3 19.3% versus 13.5% on average, respectively) than in tributaries draining the Lhasa Block (57.0% versus 61.0% and Al_2O_3 17.4% versus 14.9% on average, respectively) (Fig. 2A,B).

Along the Yarlung mainstem, CIA values tend to decrease downstream from 66 to 62 on average in suspended load and from 65 to 58 in sandbar sediment, while WIP values increase from 43 to 56 in suspended load and from 35 to 51 in sandbars. Sediments from Himalayan tributaries show CIA values ranging from 62 to 71 in suspended load and from 64 to 67 in sandbars, whereas Lhasa Block sediments range from 54 to 62 in suspended load and from 52 to 59 in sandbars. WIP values range from 50 to 57 in suspended load and from 41 to 44 in sandbars of Himalayan tributaries, and from 62 to 81 in suspended load and from 55 to 64 in sandbars of Lhasa Block tributaries (Table S2).

Alkali and alkaline-earth metals in both suspended load and sandbars display the mobility sequence: Na > Ca > Sr > Mg > Ba > K ≈ Rb, with α^{Al}_{Na} ranging from 1.0 to 3.4 and α^{Al}_{Ca} varying more irregularly from 0.5 to 4.8 because of the local presence of carbonate grains (Fig. 2).

DISCUSSION

Suspension sorting effect

The chemical composition of sediments is crucially dependent on the partitioning of minerals with different size, density, and shape in the water column (e.g., Slingerland, 1984). Suspended mud is enriched in slow-settling phyllosilicates, and consequently in Al, K, and Rb, whereas bedload sand is enriched in tectosilicates and heavy minerals, and consequently in Si, Na, Ca, and Sr (Garzanti *et al.*, 2011). The Al/Si ratio, well established as a grain-size proxy, is observed to systematically increase upwards in fluvial channels from tectosilicate-rich bedload to phyllosilicate-rich suspended load (Bouchez *et al.*, 2011; Lupker *et al.*, 2011; Guo *et al.*, 2018). In the Yarlung catchment, the Al/Si ratio is 0.31 to 0.50 in suspended mud, mostly <0.22 in sandbar sand, and only slightly higher in the mud fraction contained in sandbars (from 0.21 to 0.26, reaching 0.33 in one

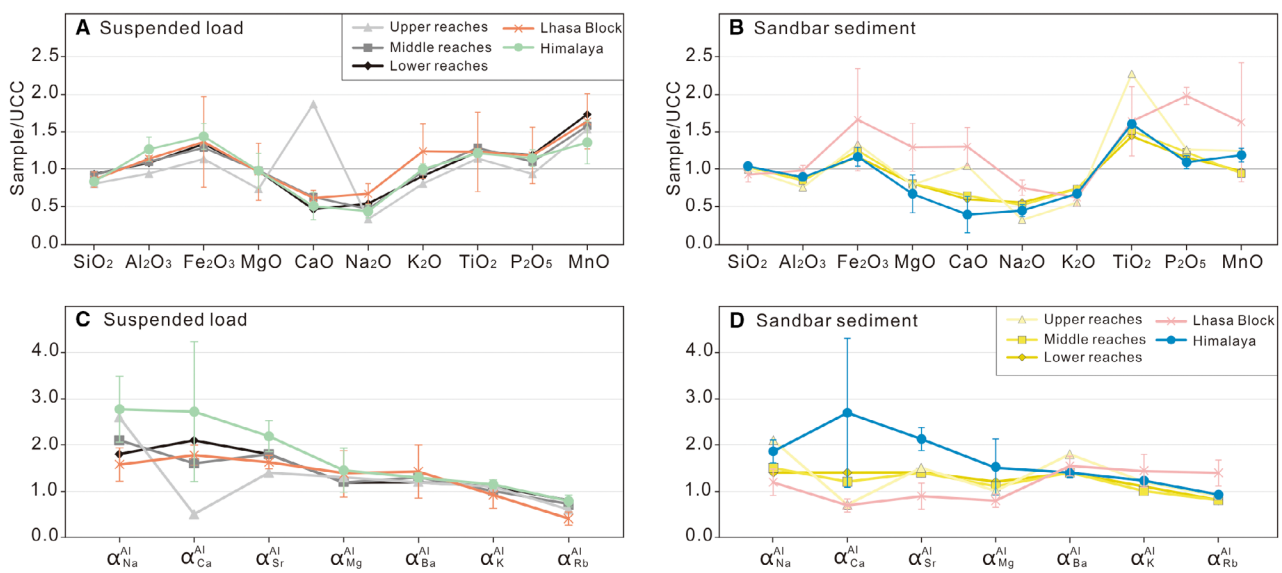

Fig. 2. Chemical composition and α^{Al} weathering indices in suspended load (A, C) and sandbars (B, D) of the Yarlung River.

Lhasa Block tributary) (Fig. 3). The chemical composition of siliciclastic detritus is thus strongly grain-size dependent, even the <63 μm fraction being finer grained in suspended sediments than in sandbar sediments.

Chemical parameters considered to be proxies of weathering are sensitive to such hydraulic-sorting processes. Notably affected are for instance the CIA, α^{Al}_{Na} (Fig. 3) and Rb/Sr ratio (Fig. S1), widely considered as proxies for weathering and pedogenic intensity (Chen *et al.*, 1999; Yang *et al.*, 2004; Bouchez *et al.*, 2011) but in fact markedly higher in suspended load than in bedload independently of weathering intensity. Whereas previous studies inferred weak to moderate weathering in the Yarlung catchment (Zhang *et al.*, 2021; Huyan *et al.*, 2022), the present study underscores that the chemical indices would point for instance at moderate weathering for suspended mud along the Yarlung mainstem, but at weak weathering for mud in sandbars (Fig. 3).

Sensitivity to grain size and climatic variation

Evaluating grain-size control on weathering indices is crucial to correctly interpret weathering signals. Our data reveal that significant differences exist between tributaries draining the Lhasa Block, where Al/Si correlates very well with both CIA (R^2 0.92) and α^{Al}_{Na} (R^2 0.93), and tributaries draining the Himalayan belt, where Al/Si correlates very poorly with CIA (R^2 0.04) and α^{Al}_{Na} (R^2 0.28) (Fig. 3). First-cycle sediments thus appear to be strongly influenced by grain-size and suspension-sorting effects, whereas these relationships are blurred by extensive recycling (Fig. 3).

Being controlled by both temperature (Deng *et al.*, 2022; Li *et al.*, 2022) and precipitation (Guo *et al.*, 2022), silicate weathering is notably sensitive to climate change (Gislason *et al.*, 2009). To investigate such effect in the Yarlung catchment, we compiled the observed mean annual temperature (MAT) and precipitation (MAP) data over the past decade (Muñoz, 2019; Peng, 2024; Fig. 1C,D).

The chemical composition of suspended mud shows only weak correlations with MAT and MAP, plausibly because of short-term transport during discrete flood events, whereas sandbar muds exhibit distinct climatic control, possibly integrating decadal-scale sedimentation. In sandbar sediments, the CIA and α^{Al}_{Na} show a weak positive correlation with MAT and a significant positive correlation with MAP for tributaries draining the Lhasa Block (Fig. 4). For Himalayan tributaries, instead, only α^{Al}_{Na} shows a slightly positive relationship with MAT (Fig. 4C) and MAP (Fig. 4D). A similar relationship is observed for Rb/Sr (Fig. S2). Largely first-cycle sediments generated from the Lhasa Block thus reflect true weathering conditions far better than sediments recycled from Tethys Himalayan sedimentary rocks.

The current temperature and precipitation conditions fail to be faithfully recorded in the chemical composition of recycled sediments from the Tethys Himalaya. In the absence of significant differences in MAT and MAP, sediment generated in the Lhasa Block yields significantly

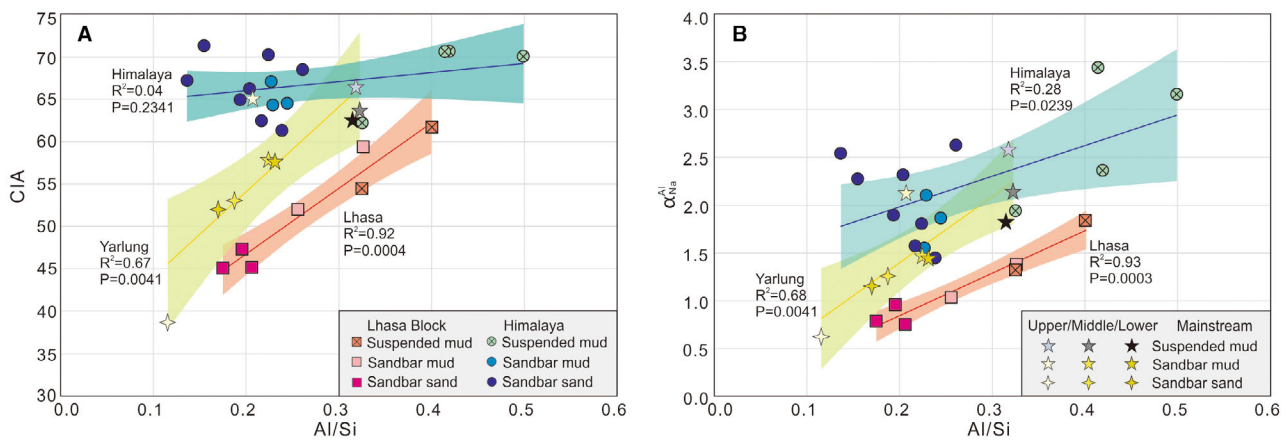

Fig. 3. Grain-size effect on CIA (A) and α^{Al}_{Na} (B) values.

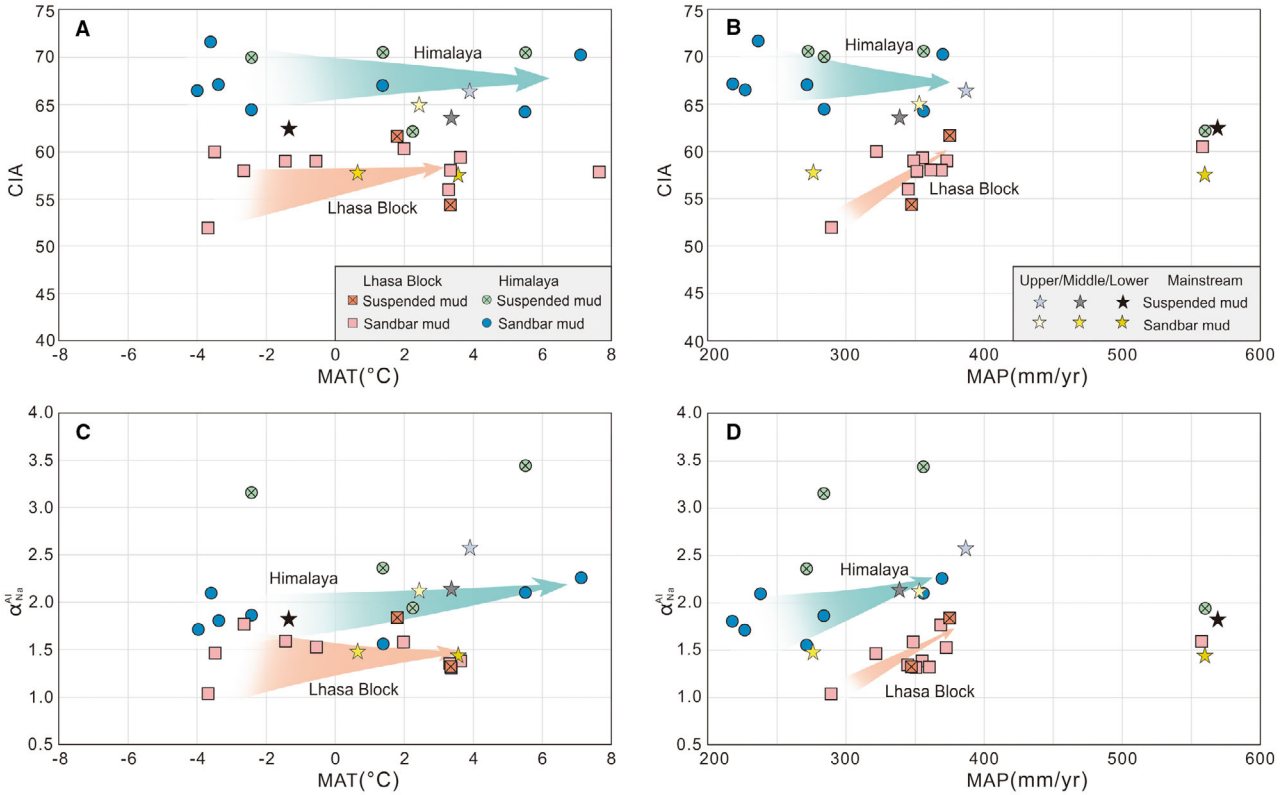

Fig. 4. Comparison between chemical weathering indices and average annual temperature and precipitation in the Yarlung catchment. Location of eight sandbar muds from Lhasa Block and four sandbar muds from Himalaya (Yu *et al.*, 2025; Zhao *et al.*, 2025) indicated in Fig. 1D.

lower weathering indices (CIA 52 to 62; α^{Al}_{Na} 1.0 to 1.8) than sediment generated in the Himalayan belt (CIA 62 to 71; α^{Al}_{Na} 1.6 to 3.4). The reliability of temperature estimates based on chemical indices (e.g., the CIA is widely used to infer average annual temperatures, with an increase estimated as 0.8 to 1.0 CIA unit/°C; Li *et al.*, 2022; Deng *et al.*, 2022) must thus be questioned (Fig. 4). Provenance effects, and specifically the influence of inherited weathering by recycling, should be duly considered when reconstructing paleo-temperatures using chemical indices.

Differences in weathering indices between first-cycle and recycled sediments

High CIA values and low WIP values are generally intended to indicate stronger weathering intensity. The CIA index, however, is notably influenced by source-rock lithology, grain size, and hydraulic sorting (Garzanti & Resentini, 2016), whereas the WIP merely measures the amount of a set of mobile elements that decrease rapidly wherever quartz is added to the sediment, and should thus be considered as an index of quartz recycling more than an index of weathering (Garzanti *et al.*, 2013; Dinis *et al.*, 2017; Guo *et al.*, 2018).

In the Yarlung catchment, Lhasa Block sediments consistently display lower CIA and higher WIP values than Himalayan sediments in corresponding grain-size fractions (Fig. 5A,C). The CIA is typically <60 (excepting clay fractions) in Lhasa Block sediments and mostly >60 in Himalayan sediments (Fig. 5A). The WIP is >50 in first-cycle sediments generated in the Lhasa Block but <50 in recycled sediments from the Himalayan belt (Fig. 5A), where the WIP is higher in suspended mud depleted in quartz and enriched in phyllosilicates (and hence especially in K). Across all grain-size fractions, the α^{Al}_{Na} values are lower in Lhasa Block sediments than in Himalayan sediments (Fig. 5B), the former ranging from 0.7 to 1.8 (but from 4.0 to 5.0 in clay fractions) and the latter from 1.6 to 3.6

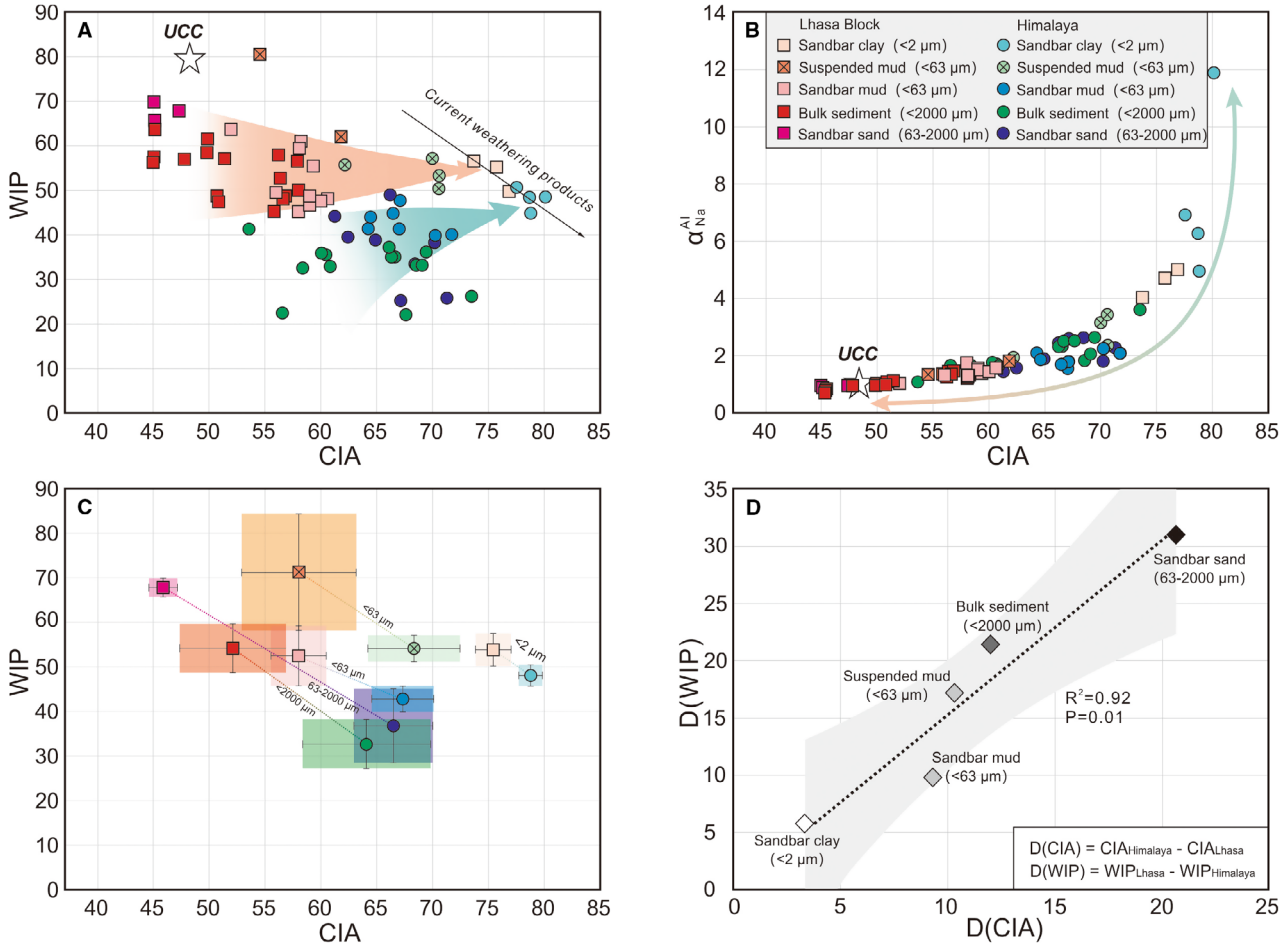

Fig. 5. Comparison of weathering indices in sediment generated from the Himalayan belt and Lhasa Block. Coloured boxes (panel C) represent mean CIA and WIP values with ±1 standard deviation. D(CIA) and D(WIP) are differences in CIA and WIP values between Himalayan and Lhasa Block sediments.

(but from 5.0 to 11.9 in clay fractions). Even weathering indices like CIA and α^{Al}_{Na} are largely independent of quartz addition; they are still affected by the inherited weathering signals from the recycling process (Guo *et al.*, 2018; Garzanti *et al.*, 2022, 2025b).

The CIA/WIP versus CIQ diagram has been proposed to distinguish the influences of weathering intensity, hydrodynamic sorting and sedimentary recycling (Guo *et al.*, 2024). The CIQ values of suspended samples from the Lhasa Block and Himalaya tributaries are concentrated around 0, indicating negligible quartz dilution. In Lhasa Block sandbar sediments, mud fractions exhibit lower CIQ values (0.29 to 0.32) and higher CIA values (52 to 59), whereas sand fractions show higher CIQ values (0.36 to 0.46) and lower CIA values (45 to 47) due to the hydrodynamic sorting effect (Fig. 6). The CIA/WIP ratio is an effective tool for assessing the first-cycle and recycled sediments (Garzanti *et al.*, 2013; Guo *et al.*, 2024). The Lhasa Block sediments consistently exhibit lower CIA/WIP values than Himalayan sediments in suspended loads (0.7 to 1.0 versus 1.2 to 1.4), mud fractions (0.8 to 1.1 versus 1.5 to 1.6) and sand fractions (0.6 to 0.7 versus 1.3 to 2.8) (Fig. 6). The broader and higher CIQ and CIA/WIP values in Himalayan sediments both reflect the influence of previous sedimentary cycles (Fig. 6).

Sand tends to contain more unweathered detritus than mud, and its geochemical signature is thus controlled to a greater extent by source-rock lithologies (e.g., Nesbitt *et al.*, 1996; Garzanti *et al.*, 2025a). The contrasting weathering indices in river sediments of igneous and

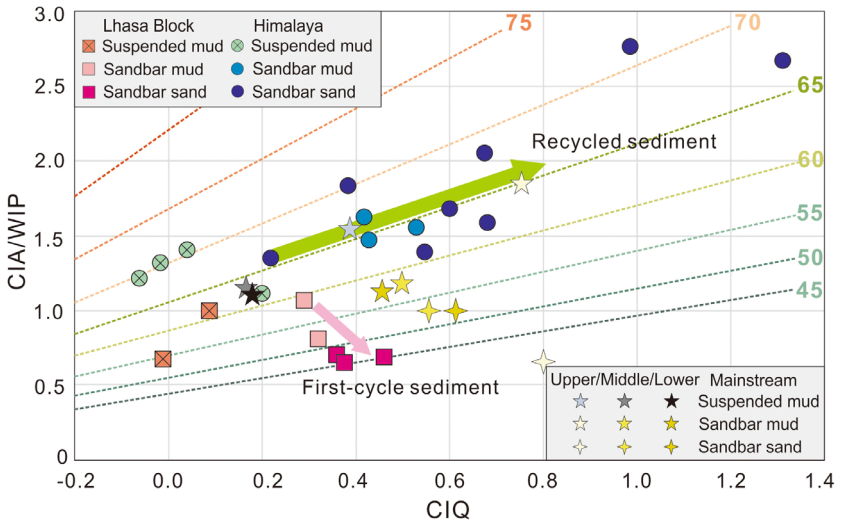

Fig. 6. CIA/WIP versus CIQ values. The diagram after Guo *et al.* (2024).

sedimentary rocks in the Yarlung River catchment show that even the geochemical composition of mud (<63 μm) is largely influenced by the lithology of source rocks (Fig. 5). This can be further supported by the effect of lithology on the composition of silt-sized sediments (Fu *et al.*, 2025). The differences D(CIA) and D(WIP) between Himalayan and Lhasa Block sediments correlate quite well with grain size (R^2 0.92), which is chiefly interpreted as a recycling effect. Differences decrease with decreasing grain size, but remain significant even for clay (<2 μm fraction; Fig. 5D; Table S3).

Comparison with the global geochemical database

A more general approach to assess the recycling effect on the CIA and WIP values was based on the inspection of a global geochemical database for river sediments (Deng *et al.*, 2022). It is well known that climate is the main factor controlling the chemical weathering process (Deng *et al.*, 2022; Guo *et al.*, 2022). However, lithological differences can also significantly impact weathering assessments, especially in case of weak chemical weathering. To minimise the influence of climate, we compared differences of weathering indicators in sediments largely recycled from siliciclastic rocks (n = 1272) versus sediments largely derived first-cycle from felsic-intermediate rocks (n = 130) within 2°C average temperature intervals (Fig. 7A) and 0.1 m/year average precipitation intervals (Fig. 7B). The relationship between CIA and MAT or MAP is clear for first-cycle detritus (Perri, 2020) but blurred for recycled sediments, which is chiefly explained by the incorporation of chemical alteration inherited from previous sedimentary cycles (Fig. 7).

Under low-temperature and low-precipitation conditions, sediments generated in catchments dominated by siliciclastic rocks typically exhibit higher CIA (Fig. 7) and lower WIP values (Fig. S3) than those derived in larger proportion from felsic-intermediate igneous rocks. Although weathering signatures in the same temperature or precipitation intervals are influenced by other factors, including runoff, elevation, and soil depth (Li & Yang, 2010; Xu *et al.*, 2023), the available data indicate that when the average annual temperature is <16°C, the CIA index in largely recycled sediments exceeds by >3 units that in largely first-cycle sediments. At the lowest annual temperatures, such a difference in CIA values reaches 10 (2 to 4°C) or even 20 units (−4 to −2°C) (Fig. 7A). Moreover, the CIA values of recycled sediments exceed those of first-cycle sediments under most precipitation conditions, a difference that reaches 10 to 20 units when the annual precipitation is <0.7 m/year (Fig. 7B). The average difference in WIP values also decreases with increasing weathering intensity, being of 13 to 15 units at annual temperatures <16°C, and of 5 to 24 units at different annual precipitation conditions (Fig. S3).

In the Yarlung catchment, where the average annual temperature is <10°C and the annual precipitation is <0.6 m/year, the CIA and WIP

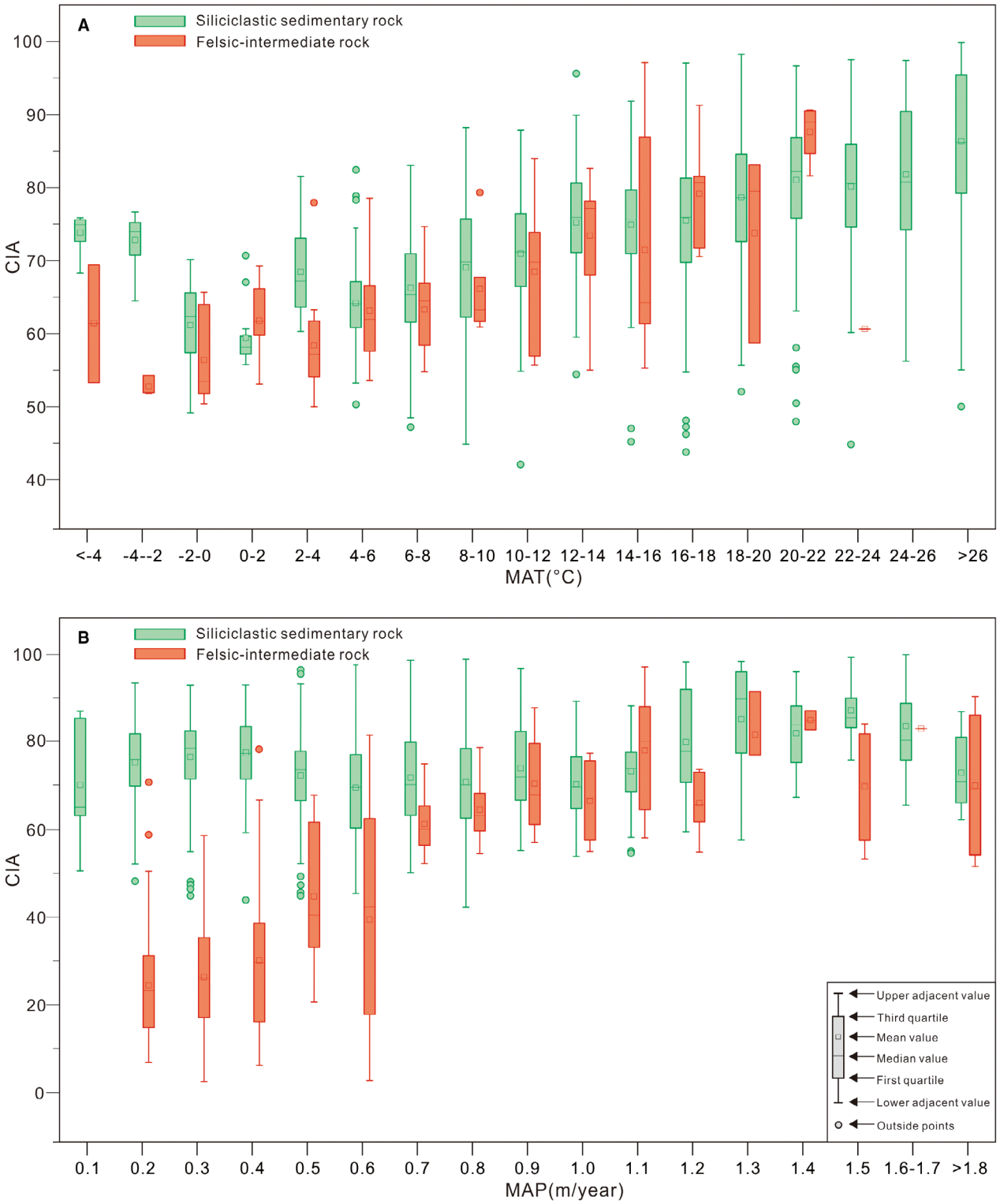

Fig. 7. Recycling effect on CIA values. Compiled CIA data are binned by MAT (A) and MAP intervals (B). Data for <63 μm fractions of bedload sediments from Deng *et al.* (2022; n = 1391); data for <63 μm fractions of sandbar and suspended sediments from this study (n = 11). Note that all these catchments are small- and median-sized (Deng *et al.*, 2022), and only catchments dominated by siliciclastic rocks or by felsic-intermediate igneous rocks – with the sum of these two lithologies exceeding 80% and the difference between the two lithologies exceeding 50% – were selected (Table S4).

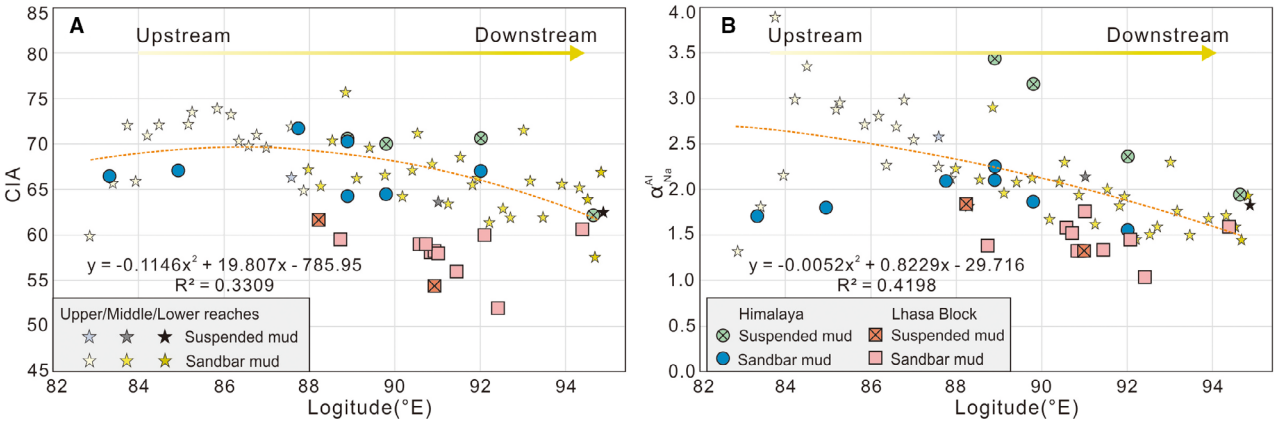

Fig. 8. Provenance effect on weathering indices. CIA (A) and α^{Al}_{Na} (B) values (from Yu *et al.*, 2025, n = 40; Zhao *et al.*, 2025, n = 5; and this study, n = 17) decrease downstream the Yarlung River because of increasing supply of first-cycle detritus from the Lhasa Block.

values are ~10 units higher in mud (<63 μm) from Himalayan sedimentary rocks than in mud from Lhasa Block granitoids and Linzizong volcanic rocks (Fig. 5D), consistently with global patterns (Fig. 7). We conclude that only first-cycle sediments can faithfully reflect the current weathering intensity. Recycled sediments, instead, commonly display markedly higher weathering indices in low temperature and precipitation conditions, thus chiefly reflecting paleo-weathering. As temperature and precipitation progressively increase, the current weathering intensity gradually becomes strong enough to override inherited paleo-weathering signals.

Recycling influence on chemical indices

Because of the semiarid climate and mild relief in Tibet, the Yarlung catchment is characterised by quite low erosion rates despite its high elevation (Liang *et al.*, 2022; Zhang *et al.*, 2022). The erosional regime was thus considered supply-limited (Yu *et al.*, 2021), with low physical erosion in the upstream areas of the Gyaca knickpoint and high in the downstream areas (Zhang *et al.*, 2022). Although temperatures and precipitation increase downstream (Fig. 1), the CIA and α^{Al}_{Na} values of mainstem sediments tend to decrease (Fig. 8). Such a trend is thus unrelated to climatic conditions and chiefly controlled by provenance. Recycled sediments supplied by Himalayan tributaries have notably higher CIA and α^{Al}_{Na} values than largely first-cycle sediments supplied by Lhasa Block tributaries. Detritus is predominantly supplied from the Himalayan belt in the upper reaches, whereas increasing amounts of detritus from the Lhasa Block are supplied to the middle and lower reaches (Liang *et al.*, 2022, 2025), thus explaining the observed decrease of CIA and α^{Al}_{Na} values downstream the Yarlung River (Fig. 8). The provenance effect highlighted above is entangled with the grain-size effect, because sediment generated in the Lhasa Block is sand-rich (Liang *et al.*, 2022), whereas sediment from the Himalayan belt is mud-rich (Liang *et al.*, 2025). Sand and mud in the Yarlung mainstem thus mainly reflect Lhasa Block and Himalayan signatures, respectively. Detritus recycled from siliciclastic rocks, including siltstone and shale, is markedly finer than detritus shed by granitoid rocks, which enhances the compositional differences between suspended mud and bedload sand observed in the Yarlung River (Liang *et al.*, 2025).

It must be noted that all major rivers flow for a substantial part of their course along sedimentary basins and that purely first-cycle sediment can consequently exist only locally in their upper reaches. Recycled sediment is invariably overwhelming (Blatt, 1967; Garzanti *et al.*, 2019), which implies that the weathering signal in all deltaic to turbiditic sediments worldwide is inevitably the sum of weathering acquired in the catchment and of paleo-weathering inherited from previous sedimentary cycles. Detangling the two effects is crucial if reliable climatic and

paleoclimatic reconstructions have to be obtained, which poses a major challenge in sedimentary research.

CONCLUSIONS

The recycling effect significantly influences the geochemical indices widely used to infer weathering intensity, thus potentially leading to gross mistakes in the evaluation of current weathering conditions in a sedimentary basin. This occurs because geochemical indices do not only incorporate the weathering signal acquired under penecontemporaneous climatic conditions (e.g., temperature and precipitation) but also the effects of paleo-weathering (i.e., all chemical effects acquired during previous sedimentary cycles). This poses a fundamental challenge in sedimentary and paleoclimatic research, because all major rivers flow for a substantial part of their course along sedimentary basins, and recycled sediment is therefore invariably abundant to overwhelming in all deltaic to turbiditic sediments and sedimentary rocks worldwide.

The Yarlung River serves as one exemplary case to demonstrate how weathering assessments may be strongly misled by diverse grain-size, lithological, and provenance controls. In the Yarlung catchment, weathering indices of largely first-cycle sediments derived from magmatic rocks of the Lhasa Block reflect the low-weathering conditions in semiarid Tibet much more faithfully than sediments recycled from the Himalayan belt, which incorporate a significant inherited component. Because of such a contrast, the variability of weathering indices across the Yarlung catchment– where climatic conditions are rather homogeneous– is chiefly controlled by the varying proportions of sediment supplied from the Lhasa Block and from the Himalaya belt, and by the notably finer grain size of Himalayan-derived sediment, i.e., by provenance rather than by climatic change.

Global data show that systematic differences in weathering indices exist between first-cycle and recycled sediments generated in the same climatic regime, and that such differences are greater under low temperature and low precipitation conditions. Detangling current weathering effects from inherited weathering effects is of essence if reliable climatic and paleoclimatic reconstructions must be obtained.

ACKNOWLEDGEMENTS

This study was supported financially by the National Natural Science Foundation of China (Grant No. 42202112) and the Second Tibetan Plateau Scientific Expedition and Research Program (STEP, Grant No. 2019QZKK0204). We thank Liu Zhifei for his careful editorial handling, and Jian Xing and another anonymous reviewer for their constructive comments and helpful suggestions.

DECLARATION OF COMPETING INTEREST

The authors declare that they have no known competing financial interests or personal relationships that could have appeared to influence the work reported in this paper.

DATA AVAILABILITY STATEMENT

The data that supports the findings of this study are available in the supplementary material of this article.

REFERENCES

An, W., **Hu, X.**, **Garzanti, E.**, **BouDagher-Fadel, M.K.**, **Wang, J.** and **Sun, G.** (2014) Xigaze forearc basin revisited (South Tibet): Provenance changes and origin of the Xigaze Ophiolite. *GSA Bull.*, **126**, 1595–1613.

Blatt, H. (1967) Provenance determinations and recycling of sediments. *J. Sed. Petrol.*, **37**, 1031–1044.

Bluth, G. and **Kump, L.R.** (1994) Lithologic and climatologic controls of river chemistry. *Geochim. Cosmochim. Acta*, **58**, 2341–2359.

Bookhagen, B. and **Burbank, D.W.** (2006) Topography, relief, and TRMM-derived rainfall variations along the Himalaya. *Geophys. Res. Lett.*, **33**, L08405.

Borges, J.B., **Huh, Y.**, **Moon, S.** and **Noh, H.** (2008) Provenance and weathering control on river bed sediments of the eastern Tibetan Plateau and the Russian Far East. *Chem. Geol.*, **254**, 52–72.

Bouchez, J., **Gaillardet, J.**, **Francee-Lanord, C.**, **Maurice, L.** and **Dutra-Maia, P.** (2011) Grain size control of river suspended sediment geochemistry: clues from Amazon River depth profiles. *Geochem. Geophys. Geosyst.*, **12**, Q03008.

Carosi, R., **Montomoli, C.**, **Iaccarino, S.** and **Visonà, D.** (2019) Structural evolution, metamorphism and melting in the Greater Himalayan Sequence in central-western Nepal. *Geol. Soc. Spec. Publ.*, **483**, 305–323.

Chen, J., **An, Z.** and **Head, J.** (1999) Variation of Rb/Sr ratios in the loess-paleosol sequences of central China during the Last 130,000 years and their implications for monsoon paleoclimatology. *Quat. Res.*, **51**, 215–219.

Clift, P.D., **Wan, S.** and **Blusztajn, J.** (2014) Reconstructing chemical weathering, physical erosion and monsoon intensity since 25 Ma in the northern South China Sea: a review of competing proxies. *Earth Sci. Rev.*, **130**, 86–102.

Dellinger, M., **Bouchez, J.**, **Gaillardet, J.**, **Faure, L.** and **Moureau, J.** (2017) Tracing weathering regimes using the lithium isotope composition of detrital sediments. *Geology*, **45**, 411–414.

Deng, K., **Yang, S.** and **Guo, Y.** (2022) A global temperature control of silicate weathering intensity. *Nat. Commun.*, **13**, 1781.

Dinis, P., **Garzanti, E.**, **Vermeesch, P.** and **Huvi, J.** (2017) Climatic zonation and weathering control on sediment composition (Angola). *Chem. Geol.*, **467**, 110–121.

von Eynatten, H., **Tolosana-Delgado, R.**, **Karius, V.**, **Bachmann, K.** and **Caracciolo, L.** (2016) Sediment generation in humid Mediterranean setting: grain-size and source-rock control on sediment geochemistry and mineralogy (Sila Massif, Calabria). *Sed. Geol.*, **336**, 68–80.

Fedo, C.M., **Nesbitt, H.W.** and **Young, G.M.** (1995) Unraveling the effects of potassium metasomatism in sedimentary rocks and paleosols, with implications for paleoweathering conditions and provenance. *Geology*, **23**, 921–924.

Fu, H., **Jian, X.** and **Pan, H.** (2023) Bias in sediment chemical weathering intensity evaluation: a numerical simulation study. *Earth Sci. Rev.*, **246**, 104574.

Fu, H., **Jian, X.**, **Zhang, Z.** and **Pan, H.** (2025) Source-rock, grain-size, weathering, and recycling controls on the feldspar/quartz ratio in silt-sized sediments. *Paleogeogr. Paleoclimatol. Paleoecol.*, **660**, 112700.

Gaillardet, J., **Dupré, B.** and **Allègre, C.J.** (1999) Geochemistry of large river suspended sediments: silicate weathering or recycling tracer? *Geochim. Cosmochim. Acta*, **63**, 4037–4051.

Garzanti, E. and **Resentini, A.** (2016) Provenance control on chemical indices of weathering (Taiwan river sands). *Sed. Geol.*, **336**, 81–95.

Garzanti, E., **Andò, S.**, **France-Lanord, C.**, **Galy, V.**, **Censi, P.** and **Vignola, P.** (2011) Mineralogical and chemical variability of fluvial sediments. 2. Suspended-load silt (Ganga–Brahmaputra, Bangladesh). *Earth Planet. Sci. Lett.*, **302**, 107–120.

Garzanti, E., **Padoan, M.**, **Setti, M.**, **Peruta, L.**, **Najman, Y.** and **Villa, I.M.** (2013) Weathering geochemistry and Sr–Nd isotope fingerprinting of equatorial upper Nile and Congo muds. *Geochem. Geophys. Geosyst.*, **14**, 292–316.

Garzanti, E., **Vermeesch, P.**, **Vezzoli, G.**, **Andò, S.**, **Botti, E.**, **Limonta, M.**, **Dinis, P.**, **Hahn, A.**, **Baudet, D.**, **De Grave, J.** and **Yaya, N.K.** (2019) Congo River sand and the equatorial quartz factory. *Earth Sci. Rev.*, **197**, 102918.

Garzanti, E., **Pastore, G.**, **Stone, A.**, **Vainer, S.**, **Vermeesch, P.** and **Resentini, A.** (2022) Provenance of Kalahari Sand: paleoweathering and recycling in a linked fluvial-aeolian system. *Earth Sci. Rev.*, **224**, 103867.

Garzanti, E., **Bayon, G.**, **Dinis, P.**, **Barbarano, M.**, **Pastore, G.**, **Vezzoli, G.**, **Braquet, N.** and **Overare, B.** (2025a) Weathering in the West Africa Craton: mineralogy and geochemistry of Niger River Sediments. *J. Geol.*, **131**, 371–409.

Garzanti, E., **Barbarano, M.**, **Dinis, P.**, **Limonta, M.**, **Pastore, G.**, **Vermeesch, P.** and **Vezzoli, G.** (2025b) Basaltic sources but quartzose sand: sediment provenance, weathering and recycling in the Uruguay River catchment. *J. Sed. Res.*, **95**, 675–692.

Gislason, S.R., **Oelkers, E.H.**, **Eiriksdottir, E.S.**, **Kardjilov, M.I.**, **Gisladottir, G.**, **Sigfusson, B.**, **Snorrason, A.**, **Elefsen, S.**, **Hardardottir, J.**, **Torssander, P.** and **Oskarsson, N.** (2009) Direct evidence of the feedback between climate and weathering. *Earth Planet. Sci. Lett.*, **277**, 213–222.

Guo, Y., **Yang, S.**, **Su, N.**, **Li, C.**, **Yin, P.** and **Wang, Z.** (2018) Revisiting the effects of hydrodynamic sorting and sedimentary recycling on chemical weathering indices. *Geochim. Cosmochim. Acta*, **227**, 48–63.

Guo, L., **Wu, J.**, **Chen, Y.**, **Xiong, S.**, **Cui, J.** and **Ding, Z.** (2022) Modern silicate weathering regimes across China revealed by geochemical records from surface soils. *Case Rep. Med.*, **127**, e2022JF006728.

Guo, Y., **Li, Y.**, **Deng, K.**, **Wang, Z.** and **Yang, S.** (2024) Decoding the signals of sediment weathering: toward a quantitative approach. *Chem. Geol.*, **651**, 122009.

Guo, Y., **Li, Y.** and **Yang, S.** (2025) The proportion of labile REEs in the river sediments serves as an index for silicate weathering intensity. *Glob. Planet. Change*, **252**, 104863.

Hameed, A. and **Srivastava, P.** (2025) Palaeopedogenesis and weathering in overbank sediments of the Siwalik Group: link to Himalayan uplift and climate change during late Miocene. *Sedimentology*, **72**, 1453–1499.

Hu, X., **Garzanti, E.**, **Moore, T.** and **Raffi, I.** (2015) Direct stratigraphic dating of India-Asia collision onset at the Selandian (middle Paleocene, 59 ± 1 Ma). *Geology*, **43**, 859–862.

Hu, X., **Garzanti, E.**, **Wang, J.**, **Huang, W.**, **An, W.** and **Webb, A.** (2016a) The timing of India-Asia collision onset – facts, theories, controversies. *Earth Sci. Rev.*, **160**, 264–299.

Hu, X., **Wang, J.**, **BouDagher-Fadel, M.**, **Garzanti, E.** and **An, W.** (2016b) New insights into the timing of the India–Asia collision from the Paleogene Quxia and Jialazi formations of the Xigaze forearc basin, South Tibet. *Gondwana Res.*, **32**, 76–92.

Huyan, Y., **Yao, W.**, **Xie, X.** and **Wang, L.** (2022) Provenance, source weathering, and tectonics of the Yarlung Zangbo River overbank sediments in Tibetan Plateau, China, using major, trace, and rare earth elements. *Geol. J.*, **57**, 37–51.

Joo, Y.J., **Madden, M.E.** and **Soreghan, G.S.** (2018) Anomalously low chemical weathering in fluvial sediment of a tropical watershed (Puerto Rico). *Geology*, **46**, 691–694.

Li, C. and **Yang, S.** (2010) Is chemical index of alteration (CIA) a reliable proxy for chemical weathering in global drainage basins? *Am. J. Sci.*, **310**, 111–127.

Li, F., **Yang, S.**, **Breecker, D.O.**, **Ramos, E.J.**, **Huang, X.**, **Duan, Z.**, **Guo, Y.**, **Li, C.** and **Mei, X.** (2022) Responses of silicate weathering intensity to the Pliocene-Quaternary cooling in East and Southeast Asia. *Earth Planet. Sci. Lett.*, **578**, 117301.

Liang, W., **Resentini, A.**, **Guo, R.** and **Garzanti, E.** (2020) Multimineral fingerprinting of modern sand generated from the Tethys Himalaya (Nianchu River, Tibet). *Sed. Geol.*, **399**, 105604.

Liang, W., **Garzanti, E.**, **Hu, X.**, **Resentini, A.**, **Vezzoli, G.** and **Yao, W.** (2022) Tracing erosion patterns in South Tibet: balancing sediment supply to the Yarlung Tsangpo from the Himalaya versus Lhasa Block. *Basin Res.*, **34**, 411–439.

Liang, W., **Hu, X.**, **Garzanti, E.**, **Dong, X.** and **Chen, F.** (2025) Contrasting provenance budgets for suspended load and bedload of the Yarlung Tsangpo, Tibet: Lhasa block or Himalaya? *Geology*, **53**, 333–337.

Lupker, M., **France-Lanord, C.**, **lavé, J.**, **Bouchez, J.**, **Galy, V.**, **Métivier, F.**, **Gaillardet, J.**, **Lartiges, B.** and **Mugnier, J.L.** (2011) A Rouse-based method to integrate the chemical composition of river sediments: application to the Ganga basin. *J. Geophys. Res.*, **116**, F04012.

McLennan, S.M. (1993) Weathering and global denudation. *J. Geol.*, **101**, 295–303.

Muñoz, S.J. (2019) ERA5-Land monthly averaged data from 1950 to present. Copernicus Climate Change Service (C3S) Climate Data Store (CDS). https://doi.org/10.24381/cds.68d2bb30.

Nesbitt, H.W. and **Young, G.M.** (1982) Early Proterozoic climates and plate motions inferred from major element chemistry of lutites. *Nature*, **299**, 715–717.

Nesbitt, H.W., **Young, G.M.**, **McLennan, S.M.** and **Keays, R.R.** (1996) Effects of chemical weathering and sorting on the petrogenesis of siliciclastic sediments, with implications for provenance studies. *J. Geol.*, **104**, 525–542.

Pan, G., **Ding, J.**, **Yao, D.** and **Wang, L.** (2004) *Geological Map of Qinghai-Xizang (Tibet) Plateau and Adjacent Areas (1:1,500,000)*. Chengdu Cartographic Publishing House, Chengdu.

Parker, A. (1970) An index of weathering for silicate rocks. *Geol. Mag.*, **107**, 501–504.

Peng, S. (2024) 1 km monthly precipitation dataset over China during 1901–2023 [Dataset]. National Earth System Science Data Center, National Science & Technology Infrastructure of China, https://doi.org/10.12041/geodata.192891852410344.ver1.db.

Perri, F. (2020) Chemical weathering of crystalline rocks in contrasting climatic conditions using geochemical proxies: an overview. *Palaeogeogr. Palaeoclimatol. Palaeoecol.*, **556**, 109873.

Rudnick, R.L. and **Gao, S.** (2003) Composition of the continental crust. In: *The Crust. Treatise on Geochemistry* (Eds Rudnick, R.L., Holland, H.D. and Turekian, K.K.), Vol. **3**, pp. 1–64. Elsevier, Oxford.

Ruxton, B.P. (1968) Measures of the degree of chemical weathering of rocks. *J. Geol.*, **76**, 518–527.

Sciunnach, D. and **Garzanti, E.** (2012) Subsidence history of the Tethys Himalaya. *Earth Sci. Rev.*, **111**, 179–198.

Shao, J., **Yang, S.** and **Li, C.** (2012) Chemical indices (CIA and WIP) as proxies for integrated chemical weathering in China: inferences from analysis of fluvial sediments. *Sed. Geol.*, **265**, 110–120.

Slingerland, R. (1984) Role of hydraulic sorting in the origin of fluvial placers. *J. Sed. Petrol.*, **54**, 137–150.

Taylor, S.R. and **McLennan, S.M.** (1995) The geochemical evolution of the continental crust. *Rev. Geophys.*, **33**, 241–265.

Wang, J., **Hu, X.**, **Garzanti, E.**, **An, W.** and **Liu, X.** (2017) The birth of the Xigaze forearc basin in southern Tibet. *Earth Planet. Sci. Lett.*, **465**, 38–47.

White, A.F. and **Brantley, S.L.** (2018) Chemical weathering rates of silicate minerals: an overview. In: *Chemical Weathering Rates of Silicate Minerals* (Eds White, A.F. and Brantley, S.L.), pp. 1–22. De Gruyter, Berlin, Germany.

Wu, W., **Zheng, H.**, **Xu, S.**, **Yang, J.** and **Yin, H.** (2012) Geochemistry and provenance of bed sediments of the large rivers in the Tibetan Plateau and Himalayan region. *Int. J. Earth Sci.*, **101**, 1357–1370.

Xu, G., **Shen, J.**, **Algeo, T.J.**, **Yu, J.**, **Feng, Q.**, **Frank, T.D.**, **Fielding, C.R.**, **Yan, J.**, **Deconink, J.F.** and **Lei, Y.** (2023) Limited change in silicate chemical weathering intensity during the Permian–Triassic transition indicates ineffective climate regulation by weathering feedbacks. *Earth Planet. Sci. Lett.*, **616**, 118235.

Yang, S., **Jung, H.S.** and **Li, C.** (2004) Two unique weathering regimes in the Changjiang and Huanghe drainage basins: geochemical evidence from river sediments. *Sed. Geol.*, **164**, 19–34.

Yang, J., **Cawood, P.A.**, **Du, Y.**, **Li, W.** and **Yan, J.** (2016) Reconstructing early Permian tropical climates from chemical weathering indices. *GSA Bull.*, **128**, 739–751.

Yu, Z., **Yan, N.**, **Wu, G.**, **Xu, T.** and **Li, F.** (2021) Chemical weathering in the upstream and midstream reaches of the Yarlung Tsangpo basin, southern Tibetan Plateau. *Chem. Geol.*, **559**, 119906.

Yu, M., **Liu, Z.**, **Zhao, Y.** and **Lin, B.** (2025) Chemical weathering and its control mechanism in the Yarlung Zangbo drainage basin on the Tibetan Plateau. *Glob. Planet. Change*, **251**, 104819.

Zhang, W., **Wu, J.**, **Zhan, S.**, **Pan, B.** and **Cai, Y.** (2021) Environmental geochemical characteristics and the provenance of sediments in the catchment of lower reach of Yarlung Tsangpo River, southeast Tibetan Plateau. *Catena*, **200**, 105150.

Zhang, X., **Xu, S.**, **Cui, L.**, **Zhang, M.**, **Zhao, Z.** and **Liu, C.** (2022) Erosions on the southern Tibetan Plateau: evidence from in-situ cosmogenic nuclides ^{10}Be and ^{26}Al in fluvial sediments. *J. Geogr. Sci.*, **32**, 333–357.

Zhao, T., **Feng, Q.**, **Yu, T.**, **Liu, W.** and **Li, B.** (2025) Geochemistry of fine sediment from small catchments reveals silicate weathering intensity and spatial variation across the Tibetan Plateau. *Catena*, **256**, 109082.

Zhu, D., **Zhao, Z.**, **Niu, Y.**, **Mo, X.**, **Chung, S.**, **Hou, Z.**, **Wang, L.** and **Wu, F.** (2011) The Lhasa Terrane: Record of a microcontinent and its histories of drift and growth. *Earth Planet. Sci. Lett.*, **301**, 241–255.

Zhu, D., **Zhao, Z.**, **Niu, Y.**, **Dilek, Y.**, **Hou, Z.** and **Mo, X.** (2013) The origin and pre-Cenozoic evolution of the Tibetan Plateau. *Gondwana Res.*, **23**, 1429–1454.

Manuscript received 27 September 2025; revision accepted 27 December 2025

Supporting Information

Additional information may be found in the online version of this article:

Figure S1. Comparison between Rb/Sr and CIA (A) and Al/Si (B) values.

Figure S2. Comparison between Rb/Sr and mean annual temperature and precipitation.

Figure S3. Recycling effect on WIP values. Compiled WIP data are binned by MAT (A) and MAP intervals (B). Data for <63 μm fractions of bedload sediments from Deng et al. (2022; n=1391); data for <63 μm

fractions of sandbar and suspended sediments from this study (n = 11).

Table S1. Sample information of the Yarlung Tsangpo sediments.

Table S2. Geochemical results and Elemental ratios.

Table S3. Values of D(CIA) and D (WIP).

Table S4. The dataset of weathering indicators, climate conditions and lithological distributions of global river sediments.